Received: 24 April 2018 | Accepted: 5 September 2018

DOI: 10.1002/hyp.13281

RESEARCH ARTICLE

WILEY

The effect of Indian Summer Monsoon rainfall on surface water δD values in the central Himalaya

Bernd Meese[1] | Bodo Bookhagen[1] | Stephanie M. Olen[1] | Frauke Barthold[1] | Dirk Sachse[1,2]

[1] Institute of Earth and Environmental Science, University of Potsdam, Germany

[2] Section 5.1, Geomorphology, GFZ German Research Centre for Geosciences, Potsdam, Germany

Correspondence
Dirk Sachse, Section 5.1, Geomorphology, GFZ German Research Centre for Geosciences, Telegrafenberg, 14473 Potsdam, Germany.
Email: dirk.sachse@gfz-potsdam.de

Funding information
Deutsche Forschungsgemeinschaft, Grant/Award Number: DFG 1364

Abstract

Stable isotope proxy records, such as speleothems, plant-wax biomarker records, and ice cores, are suitable archives for the reconstruction of regional palaeohydrologic conditions. But the interpretation of these records in the tropics, especially in the Indian Summer Monsoon (ISM) domain, is difficult due to differing moisture and water sources: precipitation from the ISM and Winter Westerlies, as well as snow- and glacial meltwater. In this study, we use interannual differences in ISM strength (2011–2012) to understand the stable isotopic composition of surface water in the Arun River catchment in eastern Nepal. We sampled main stem and tributary water (n = 204) for stable hydrogen and oxygen isotope analysis in the postmonsoon phase of two subsequent years with significantly distinct ISM intensities. In addition to the 2011/2012 sampling campaigns, we collected a 12-month time series of main stem waters (2012/2013, n = 105) in order to better quantify seasonal effects on the variability of surface water $\delta^{18}O/\delta D$. Furthermore, remotely sensed satellite data of rainfall, snow cover, glacial coverage, and evapotranspiration was evaluated. The comparison of datasets from both years revealed that surface waters of the main stem Arun and its tributaries were D-enriched by ~15‰ when ISM rainfall decreased by 20%. This strong response emphasizes the importance of the ISM for surface water run-off in the central Himalaya. However, further spatio-temporal analysis of remote sensing data in combination with stream water d-excess revealed that most high-altitude tributaries and the Tibetan part of the Arun receive high portions of glacial melt water and likely Winter Westerly Disturbances precipitation. We make the following two implications: First, palaeohydrologic archives found in high-altitude tributaries and on the southern Tibetan Plateau record a mixture of past precipitation δD values and variable amounts of additional water sources. Second, surface water isotope ratios of lower elevated tributaries strongly reflect the isotopic composition of ISM rainfall implying a suitable region for the analysis of potential δD value proxy records.

KEYWORDS

Himalaya, palaeoclimate records, snow melt, stream water, water isotopes

1 | INTRODUCTION

The stable isotopic composition of water (expressed as δD and $\delta^{18}O$ values) recorded in geological archives is often used as proxy for palaeoclimate reconstructions (e.g., Freeman & Colarusso, 2001; Johnsen, Dahl-jensen, Dansgaard, & Gundestrup, 1995; Schefuß, Ratmeyer, Stuut, Jansen, & Sinninghe Damsté, 2003; Sinha et al., 2007; Tierney et al., 2008). As precipitation δD and $\delta^{18}O$ values

 © 2018 John Wiley & Sons, Ltd.

(δD_{precip} and $\delta^{18}O_{precip}$) are influenced by factors such as the isotopic composition of moisture sources, moisture-transportation pathway, condensation temperature, and precipitation amount (Dansgaard, 1964), changes in any of these are imprinted in meteoric water δD and $\delta^{18}O$ values. Therefore, geological archives, such as speleothems (e.g., Hendy, 1971; Hendy & Wilson, 1968; Sinha et al., 2007), ice cores (e.g., Dansgaard et al., 1982; Johnsen et al., 1995), or organic matter such as plant wax biomarkers in sediments (Huang, Shuman, Wang, & Webb, 2004; Sachse, Radke, & Gleixner, 2004; Schefuß et al., 2003; Tierney et al., 2008), provide isotope proxy records indicative of past hydrologic changes. When derived from a single moisture source, recorded stable isotopes may be indicative for past precipitation amounts and temperature (Kurita, Ichiyanagi, Matsumoto, Yamanaka, & Ohata, 2009). But in the case of two or seasonally variable moisture sources with distinct isotopic compositions, the palaeoclimatic interpretation of stable isotope records is more complex (Araguás Araguás & Froehlich, 1998). Observed changes in respective isotope records can either be interpreted as a change of the dominating moisture source, changes in precipitation amount or temperature, or a combination of these factors (Lister, Kelts, Zao, Yu, & Niessen, 1991; Liu, Henderson, & Huang, 2008).

In this study, we analyse the impact of different moisture sources on stable isotope concentrations in the eastern Himalaya. The southern Himalayan front and the southern front of the Shillong Plateau are both impacted by strong, mostly ISM-derived orographic rainfall (Bookhagen & Burbank, 2006; Breitenbach et al., 2010). For the Shillong Plateau in eastern India, Breitenbach et al. (2010) showed that local ISM δD_{precip} and $\delta^{18}O_{precip}$ values mostly reflect the variability of Bay of Bengal surface water and the moisture transport history, for example, convective processes over the SE Arabian Sea (Lekshmy, Midhun, Ramesh, & Jani, 2014), with minor influence of actual rainfall amount. The southern Himalayan front is influenced by varying quantities of ISM (Bookhagen & Burbank, 2010; Hren, Bookhagen, Blisniuk, Booth, & Chamberlain, 2009; Wulf, Bookhagen, & Scherler, 2016; Yu et al., 2016), Winter Westerly Disturbances (WWD) snowfall (Sanwal et al., 2013; Smith, Bookhagen, & Rheinwalt, 2017), and glacial melt (Racoviteanu, Armstrong, & Williams, 2013; Wilson, Williams, Kayastha, & Racoviteanu, 2016). Additionally, mesoscale weather anomalies occurring along mountain ranges and plateau margins might affect δD_{precip} and $\delta^{18}O_{precip}$ values (Blisniuk & Stern, 2005; Cannon, Carvalho, Jones, & Bookhagen, 2015; Rohrmann et al., 2014).

Previous studies from the Himalayan region and the Indian subcontinent have used isotope records to reconstruct past hydrologic conditions (Berkelhammer et al., 2010; Kotlia et al., 2012; Kotlia, Singh, Joshi, & Dhaila, 2015; Liang et al., 2015; Ponton et al., 2012; Rowley, Pierrehumbert, & Currie, 2001; Sanwal et al., 2013; Sarkar et al., 2015; Sinha et al., 2005, 2011; Thompson et al., 2000). Except for Thompson et al. (2000), who analysed ice core $\delta^{18}O$ values, and Ponton et al. (2012) and Sarkar et al. (2015), who analysed terrestrial biomarkers in marine and lacustrine archives, respectively, all above cited studies used speleothem $\delta^{18}O$ records from caves located in or close to the ISM core zone and isotopic changes were interpreted as a signal of palaeo-ISM strength variability. On timescales of 10^3 years, stable isotope proxy records from within the ISM region show consistent trends from the Bølling-Ållerød to the Holocene, interpreted as insolation induced changes in ISM strength (Li, Wang, Zhou, Zhang, & Wang, 2014). However, stable isotopic variability on different timescales caused by insolation is difficult to decipher from a mixed signal. Additional complexity is added by changes of surface water $\delta^{18}O/\delta D$ values along the southern Himalayan front on short (interannual to decadal) timescales due for the following reasons: First, the imprint of convective events on atmospheric vapour while crossing the Indian subcontinent is variable. Second, the southern Himalayan front is affected by variable amounts of moisture derived from different sources (Bookhagen & Burbank, 2010; Hren et al., 2009; Wulf et al., 2016; Yu et al., 2016). Although the Himalayan front is particularly sensitive to ISM intensity (Tian et al., 2003; Yu et al., 2016), moisture source and local climate effects are poorly understood due to sparse spatio-temporal coverage of δD_{precip} and $\delta^{18}O_{precip}$ data from the northern ISM core zone.

In our study, we aim to decipher the influence of different modern moisture sources in the eastern Nepalese Himalaya on surface water δD and $\delta^{18}O$ values using a combined stable isotope and remote sensing approach. We rely on satellite remote sensing data of rainfall distribution (Tropical Rainfall Measurement Mission [TRMM] data product 3B42V7, Huffman et al., 2007), snow cover (MODIS data product MOD10C1, Hall, Riggs, Salomonson, DiGirolamo, & Bayr, 2002), and evapotranspiration (MODIS data product MOD16A2, Mu, Zhao, & Running, 2011), together with recent water δD and $\delta^{18}O$ values (2011–2012). In the Arun Valley, a strong orographic and altitude effect (Dansgaard, 1964; Gonfiantini, Roche, Olivry, Fontes, & Zuppi, 2001; Olen et al., 2015) is reflected by surface water δD and $\delta^{18}O$ values (Hoffmann et al., 2016), similar to the Kali Gandaki River 350 km to the west (Garzione, Quade, DeCelles, & English, 2000). Because multiseason δD_{precip} and $\delta^{18}O_{precip}$ records from this region are rare and difficult to obtain due to poor accessibility, we analysed surface water of the eastern Nepalese Arun River and its tributaries (Figure 1a and 1b) in two consecutive years (2011–2012) where annual monsoonal rainfall amount differed by ~20%. Additional sampling of the Arun was done every 3–4 days from October 2012 to November 2013 in order to quantify the Arun's seasonal isotopic variability. Even though the isotopic composition of stream water can be characterized by significant excursions for hours up to a few days following heavy rainfall events (Buttle, 1994; DeWalle, Edwards, Swistock, Aravena, & Drimmie, 1997; Soulsby, Malcolm, Helliwell, Ferrier, & Jenkins, 2000), δD and $\delta^{18}O$ values of stream base flow are the best estimate for catchment-wide, weighted mixture of different water sources. As such, our data from the Arun Valley provide the opportunity to evaluate how the ISM and other hydrological variables affect the isotopic composition of environmental waters, being the water source of different terrestrial organic and inorganic isotope proxy archives.

2 | GEOGRAPHIC AND CLIMATIC SETTING

The Arun catchment covers the world's steepest altitudinal gradient above the sea level ranging from 205 m asl at the confluence of the Arun, Tamur, and Sun Koshi Rivers in southern Nepal to 8848 m asl at the summit of Mount Everest. The Arun River originates on the

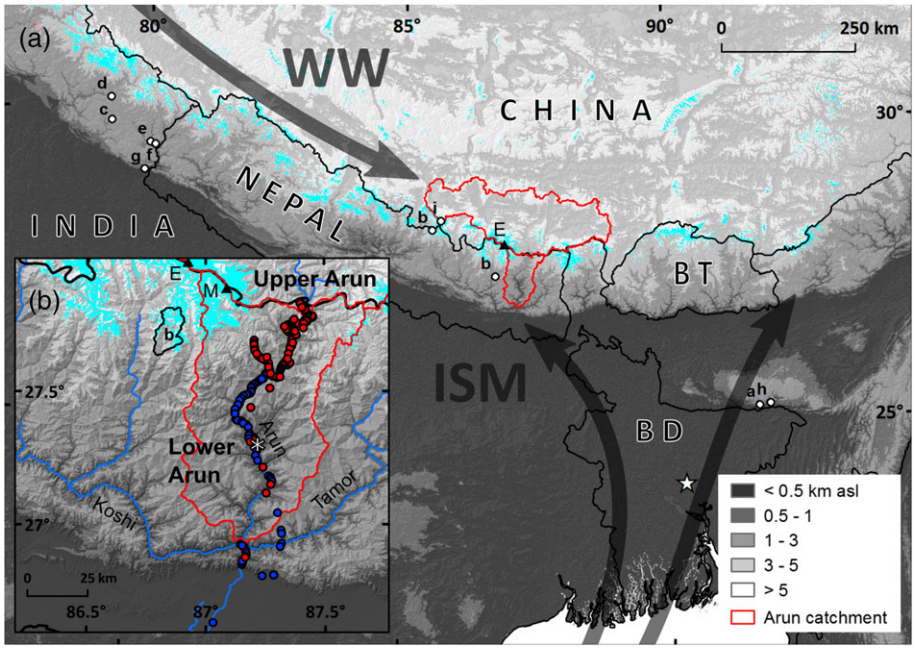

FIGURE 1 (a) Location of the Arun Valley in the eastern Nepalese Himalaya. Red polygon outlines Arun catchment, which is separated into an upper and lower Arun roughly following the Nepalese–Chinese border. Arrows indicate directions of major moisture transport (ISM: Indian Summer Monsoon; WW: precipitation from Winter Westerly disturbances), cyan denotes glaciated areas (GLIMS 2005, Global Land Ice Measurements from Space, www.glims.org), white star—Dhaka GNIP weather station, E—Mount Everest, white dots—cited (palaeo)climate studies: a—Breitenbach et al. (2010), b—Racoviteanu et al. (2013), c—Kotlia et al. (2012), d—Kotlia et al. (2015), e—Liang et al. (2015), f—Sanwal et al. (2013), g—Sinha et al. (2005), h—Sinha et al. (2011), i—Thompson et al. (2000); Yao et al. (2006). (b) Surface water sample sites (n = 204), colour indicates sampling year (blue—2011, red—2012), asterisk denotes Tumlingtar, location of time series sampling, M—Makalu

southern Tibetan Plateau in China and flows through eastern Nepal, transecting the Himalayan ranges from north to south. At its outlet in the southern Himalayan front, the Arun drains an area of 33.58 × 10^3 km^2, of which approximately 15% is located in Nepal and the remaining 85% in China, mostly on the southern Tibetan Plateau at an elevation above 3,000 m (Figure 1b). South of the confluence of the Arun, Tamur, and Sun Kosi Rivers, the river is called Sapta Koshi and joins the Ganges, subsequently draining to the Bay of Bengal. In this study, we distinguish between the lower Arun, mostly located in the Nepalese Himalaya (catchment of Arun between 206 and 1,793 m asl river elevation, ~5.26 × 10^3 km^2), and the upper Arun, mostly located on the southern Tibetan Plateau (catchment above 1,763 m asl Arun river elevation, ~28.32 × 10^3 km^2; Figure 1a). These two areas are roughly separated by the Nepalese–Chinese border (Figure 1b).

Precipitation in the Arun Valley is dominated by the Indian Summer Monsoon (ISM), originating from the Arabian Sea, crossing the Indian subcontinent and passing the Bay of Bengal (Figure 1a). The ISM affects the valley's entire watershed and contributes ~70% of its annual rain volume during the peak ISM season between June and September (Bookhagen & Burbank, 2010). In addition to the ISM, the uppermost tributaries of the lower Arun and the upper Arun receive winter precipitation in the form of WWD originating from the Caspian, Black, and Mediterranean Seas (Bookhagen & Burbank, 2010; Cannon et al., 2015; Lang & Barros, 2004), although in considerably lower amounts than from the ISM. The Arun also receives glacial melt water from glaciers covering 4.91% of its total catchment area and 4.93% and 4.84% of the upper and lower Arun, respectively (*GLIMS 2005, Global Land Ice Measurements from Space, www.glims.org*). Hence, main stem water and several high-altitude tributaries likely receive glacial melt in addition to summer and winter precipitation (Figure 1a and 1b).

The substantial interannual variability of ISM intensity is evidenced by flooding events and droughts on the Indian subcontinent during the past 150 years and beyond (Malik, Bookhagen, & Mucha, 2016; Mooley & Parthasarathy, 1984). Monsoonal intensity can be described by different indices (Parthasarathy, Rupa Kumar, & Kothawale, 1992), most commonly based on wind-system gradients. The Indian Summer Monsoon Index (IMI; Wang & Fan, 1999) describes potential air-mass mobilization from the Indian Ocean towards the Himalayan mountain range based on NCEP/NCAR reanalysis data of June–September. The dimensionless IMI is normalized to the long-term mean (1948–2015), where indices larger (less) than zero indicate an intensified (attenuated) ISM. In 2011, the first year of sampling, the IMI was −0.426 standard deviations below the long-term mean (International Pacific Research Center, University of Hawaii, http://apdrc.soest.hawaii.edu/projects/monsoon/seasonal-monidx.html), indicating an ISM slightly weaker than the 68 year-average. An IMI of −1.677 in the second year of sampling indicated a significantly weaker ISM season prior to the second sampling campaign in November 2012. In fact, only 5 years of available NCEP/NCAR reanalysis data between 1948 and 2015 yielded a lower IMI. Data from the Bangladesh GNIP (Global Network of Isotopes in Precipitation, International Atomic Energy Agency) climate station in Dhaka (Figure 1a) also indicate that the 2012 ISM was less intense than in 2011. Recorded cumulative precipitation at Dhaka limited to the ISM peak season (June–September) was 1,241 and 762 mm in 2011 and 2012, respectively (June–September mean 2009–2015: 1,147 mm, σ = 373 mm).

3 | METHODS

3.1 | Surface water sampling

In order to determine the spatio-temporal variability of surface water δD and $\delta^{18}O$ values, 204 stream samples were taken in the lower Arun in September 2011 and October/November 2012. The main focus of 2011 sampling was the southern to central section of the lower Arun Valley. 2012 sampling was focused on the central to northern part of the lower Arun (Figure 1). We resampled the main stem at two sites (four samples in total), four tributaries were sampled in both years (Table 1). On average, the Arun main stem was roughly sampled in 10-km intervals, the outlets of tributaries every 0.5 to 3 km, depending on accessibility. Five of the sampled tributaries have a glacial coverage varying from 0.5% to 36% of respective total catchment area (Table S1, online version). To create a time series of the Arun main stem signature, 105 additional water samples were taken close to the town of Tumlingtar (87.189°E, 27.311°N) every 3 to 4 days between 02/11/2012 and 10/11/2013. For sampling, gas tight 2-ml glass vials were flushed with stream water and then filled.

3.2 | Measurement of surface water δD and $\delta^{18}O$

Prior to δD and $\delta^{18}O$ measurements, all water samples were filtered through 45-μm polyethylene filters. The surface water isotopic composition was determined by laser spectroscopy on a Liquid Water Isotope Analyzer (Los Gatos Research, Mountain View, California, USA), at the Institute of Earth and Environmental Sciences, University of Potsdam. Every sample was run in six replicates; only the last four measurements were used to calculate sample means. For every fifth sample, we measured three isotope standards (δD = −154.3‰, −96.4‰, −9.5‰, respectively, Los Gatos Research water isotope standard). In order to convert D/H ratios to the Vienna Standard Mean Ocean Water–Standard Light Antarctic Precipitation scale, a least square linear regression function based on measured and known standard δD and $\delta^{18}O$ values was used. The accuracy of δD and $\delta^{18}O$ measurements is reported as one standard deviation between measured and known values of water standards (i.e., the root-mean-square error) and was 1.02‰ and 0.06‰, respectively. The precision of δD and $\delta^{18}O$ measurements is reported as one standard deviation of triplicate measurements (Tables S1 and S2, online version).

The deuterium excess *d* of sampled stream water was calculated (Dansgaard, 1964) by

$$d = \delta D - 8 * \delta^{18}O. \quad (1)$$

3.3 | Topographic and climatic raster data

For terrain analyses, the void-filled Shuttle Radar Topography Mission (SRTM V4) digital elevation model with a ground resolution of 90 m (Jarvis, Reuter, & Nelson, 2008) was used. We determined the Arun River catchment using standard geographic information system tools. For the evaluation of spatio-temporal rainfall variability, we used daily TRMM data product TRMM 3B42-V7 with 3-hr temporal resolution and a spatial resolution of 0.25° (~30 km; Bookhagen, 2010; Bookhagen & Burbank, 2010; Huffman et al., 2007). Even though the TRMM 3B42 dataset tends to over-predict rainfall at high elevation and in arid areas (Bookhagen & Burbank, 2010; Wulf et al., 2016), relative and interannual variabilities are well captured (Wulf et al., 2016). The TRMM data were bilinearly resampled to a spatial resolution of 5 km. Advanced Microwave Scanning Radiometer (AMSR-E) snow water equivalent estimations were only available until October 2011, and it could not be used for snow-melt evaluation (Tedesco, Kelly, Foster, & Chang, 2004). Instead, the spatio-temporal snow analysis is based on daily MODIS MOD10C1 snow cover data with a spatial resolution of 0.05° (~5 km) from January 2004 until the end of 2012 (Hall et al., 2002). For a detailed rationale of why MODIS snow cover data are a reasonable approach for snow melt trends during both sampling campaigns, we refer to a comparison of MODIS snow cover and AMSR snow water equivalent data in Appendix S1.

In order to evaluate the amount of evapotranspiration in the Arun Valley, we analysed MODIS MOD16A2 evapotranspiration data (Mu et al., 2011) from 2011 and 2012 with a spatial resolution of ~5 km. For more details, we refer to Appendix S2 and Figure S2.

4 | RESULTS

4.1 | Stream water δD values

Surface water δD values (δD_{sw}) of all 204 samples ranged from −109.6‰ to −36.4‰. Tributary δD_{sw} values ($\delta D_{sw,trib}$) in 2011 ranged from −92.5‰ to −42.9‰ with an average of −56.2‰ (σ = 8.5‰, n = 72), whereas they were between −84.3‰ and −36.4‰ with an average of −52.1‰ (σ = 7.6‰, n = 115) in 2012 (Figure 2a, Table S1,

TABLE 1 Replicate surface water samples

Lon	Lat	Site 2012	Site 2011	δD 2011	δD 2012	ΔD	$\delta^{18}O$ 2011	$\delta^{18}O$ 2012	$\Delta^{18}O$
87.28	27.57	**12009**	**11049**	−105.7	−88.7	17	−14.8	−12.2	2.6
87.28	27.57	**12113**	**11049**	−105.7	−91.2	14.5	−14.8	−13	1.8
87.28	27.57	**12139**	**11049**	−105.7	−91	14.7	−14.8	−12.9	1.9
87.24	27.22	12145	11080	−59.7	−46.2	13.5	−8.8	−7.2	1.6
87.28	27.15	12146	11085	−57.6	−40.1	17.5	−8.7	−6.4	2.3
87.25	27.12	12147	11086	−58.5	−45	13.5	−8.8	−6.6	2.2
87.15	26.93	12149	11100	−91.9	−76.2	15.7	−13.2	−10.9	2.3
87.15	26.93	**12150**	**11102**	−92.5	−77.5	15	−13.2	−11.1	2.1

Note. δD and $\delta^{18}O$ values are shown with offset ΔD and $\Delta^{18}O$ (Equation (2)) between both years. Main stem samples are indicated by bold sample id.

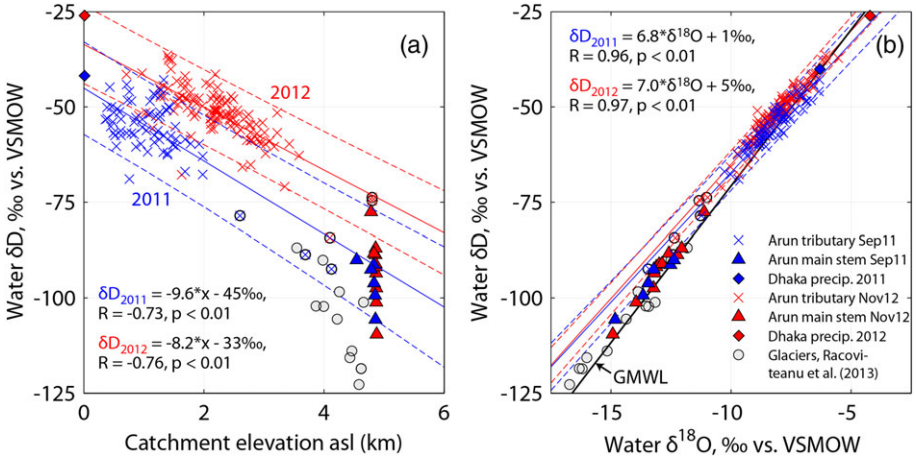

FIGURE 2 (a) Surface water δD and δ18O values separated by sample year (2011: blue, 2012: red) of the Arun main stem (triangles) and its tributaries (crosses; see Table S1, online supplement, for analytical errors). Glaciated tributaries are indicated by black circles. Linear regressions of tributary δD values (solid line) are shown together with 95% confidence intervals (dashed lines). (b) Surface water δD versus δ18O values and Global Meteoric Water Line (GMWL, black, δD = 8.2*δ18O + 11.27, Rozanski, Araguás-Araguás, & Gonfiantini, 1993), glacial melt and precipitation data from Dhaka, Bangladesh. Solid and dashed lines show linear regressions with 95% confidence intervals of 2011 and 2012 tributary data (see Table 2 for more details)

online version). The six water samples taken from five different glaciated tributary catchments were characterized by most negative $\delta D_{sw,trib}$ values (Figure 2a, Table S1, online supplement). $\delta D_{sw,trib}$ values, including those of glaciated tributaries, were inversely correlated to tributary median catchment elevation with Pearson correlation coefficients (R) of −0.73 and − 0.76 and $p < 0.01$ for years 2011 and 2012, respectively. Isotopic lapse rates were −9.56‰ km^{-1} ± 1.08‰ km^{-1} (1σ) and −8.24‰ km^{-1} ± 0.65‰ km^{-1} in September 2011 and November 2012 with intercepts of −45.0 ± 1.43‰ and −33.6 ± 1.54‰, respectively (Figure 2a, Table 2). We performed an analysis of covariance to test for significant differences between both $\delta D_{sw,trib}$-altitude relationships (lapse rates). The test revealed that slopes were not significantly different ($p = 0.27$) whereas y intercepts were ($p < 0.01$).

$\delta^{18}O_{sw,trib.}$ and $\delta D_{sw,trib}$ were correlated in both years ($R = 0.96$ and $R = 0.97$, $p < 0.01$ in 2011 and 2012, respectively) and regression functions had smaller slopes and y intercepts compared to the global meteoric water line (GMWL: $\delta D = 8.2*\delta^{18}O + 11.27$, Rozanski et al., 1993; Figure 2b, Table 2). The slopes of $\delta^{18}O_{sw,trib.}$ /$\delta D_{sw,trib.}$ Linear regressions in both years were similar within the range of statistical errors, but intercepts differed (Table 2).

Arun main stem δD_{sw} values ($\delta D_{sw,Arun}$) in September 2011 ranged from −105.7‰ to −90.1‰ (mean = −95.8‰, σ = 5.9‰, n = 6) and in November 2012 from −109.6‰ to −77.5‰ (mean = −92.5‰, σ = 8.3‰, n = 11; Figure 2a). An analysis of covariance test comparing lapse rates from both years was not applied, because the precondition of linear correlation between $\delta D_{sw,Arun}$ and catchment elevation was not fulfilled for the 2011 samples.

For interannual comparison of replicate water samples, $\Delta D_{2011/2012}$ was calculated by ordinary differences:

$$\Delta D_{2011/2012} = \delta D_{sw,2011} - \delta D_{sw,2012,} \quad (2)$$

where $\delta D_{sw,2011}$ and $\delta D_{sw,2012}$ are samples taken at the same spot during both sampling campaigns (Table 1). For the four main stem replicate samples taken at two different sites, the mean $\Delta D_{2011/2012}$ was 15.3‰ (σ = 1.2‰; Table 1). Tributary mean $\Delta D_{2011/2012}$ (n = 4) was 15.1‰ (σ = 1.9‰). $\Delta^{18}O_{2011/2012}$ was calculated similarly to $\Delta D_{2011/2012}$ (Equation (2)) and amounts to mean values of 2.1‰ (σ = 0.3‰) for both main stem and tributary samples. The total mean $\Delta D_{2011/2012}$ ($\Delta^{18}O_{2011/2012}$) including main stem and tributary samples was 15.2‰ (2.1‰) with one standard deviation of 1.5‰ (σ = 0.3‰; n = 8).

Time series samples ($\delta D_{sw,ts}$) of the Arun main stem ranged from −100.4‰ to −45.2‰, taken on 29/05/2013 and 29/10/2013, respectively (Figure 4a, see Table S2, online supplement, for respective $\delta^{18}O_{sw,ts}$). Late autumn/early winter (mid-November–end December 2012) was a period with a notable $\delta D_{sw,ts}$ value drop below the overall annual mean of −81‰ reaching values between −100‰ and −90‰.

TABLE 2 Least square linear regression results of surface water δD values with median catchment elevation in km asl (elev.) and $\delta^{18}O$

Variables	Year	Regression function	R	p
δD vs. elev.	2011	$\delta D_{sw,trib}$ = elev. *−9.56 (±1.08) − 45.0 (±1.43)	−0.73	<0.01
δD vs. elev.	2012	$\delta D_{sw,trib}$ = elev. *−8.24 (±0.65) − 33.6 (±1.54)	−0.76	<0.01
δD vs. $\delta^{18}O$	2011	$\delta D_{sw,trib.}$ = $\delta^{18}O_{sw,trib.}$ *6.79 (±0.23) + 0.72 (±1.91)	0.96	<0.01
δD vs. $\delta^{18}O$	2012	$\delta D_{sw,trib.}$ = $\delta^{18}O_{sw,trib.}$ *7.01 (±0.16) + 4.99 (±1.30)	0.97	<0.01
d-excess vs. elev.	both years	d = x *1.52 (±0.19) + 9.49 (±0.38)	0.48	<0.01

Note. Additionally, the regression function of d-excess (both years combined) and median catchment elevation (elev.) is given. Standard deviation of slope and intercept are provided as well as Pearson's correlation coefficients R and p value.

Opposed to the trough in early winter, $\delta D_{sw,ts}$ values peak between the middle of February and middle of April with values ranging from −78‰ to −46‰. Between 11/9/2013 and 29/10/2013, five samples with −49‰ to −45‰ were collected. Each of these samples is isolated and framed by several $\delta D_{sw,ts}$ values around −85‰.

4.2 | Stream water deuterium excess

Deuterium excess (*d or d-excess*) of September 2011 tributary water ranged from 4.8 ± 0.8‰ to 15.5 ± 1.6‰ (mean 10.9‰, one standard deviation σ = 2.7‰, n = 72). In November 2012, tributary d-excess was in between 7.2 ± 3.0‰ and 20.3 ± 4.5‰ (mean 13.0‰, σ = 2.0‰, n = 115; Figure 3). Average d-excess of replicate tributary samples from November 2012 and September 2011 were statistically similar (Δd = −1.8‰, σ = 2.1‰, n = 4). d-Excess was not correlated to catchment elevation for 2011 and 2012 datasets separately, but combined d-excess from both years yielded a significant correlation to median catchment elevation (R = 0.48, p < 0.01; Figure 3). Least square linear regression yielded a slope of 1.52‰ km^{-1} and an intercept of 9.49‰ (Table 2). However, above 2.5-km median catchment elevation deuterium excess did not increase anymore.

Arun main stem water samples covered a comparable d-excess range during both sampling campaigns ranging from 8.8‰ to 13.2‰ in 2011 (mean = 11.0‰, σ = 1.6‰, n = 6) and 8.4‰ to 13.0‰ in 2012 (mean = 10.9‰, σ = 1.9‰, n = 11). Replicate main stem d-excess did not differ significantly (Δd = 1.7‰, σ = 1.5‰, n = 4). We did not observe a correlation between median catchment elevation and the Arun's main stem d-excess, neither for both years individually, nor for the combined 2011 and 2012 data.

d-Excess of Arun time series samples from Tumlingtar did not show an obvious temporal distribution as $\delta D_{sw,ts}$ values (cf. Figure 4a and 4b). We calculated running mean d-excess using a Gaussian 15 day-filter in order to visualize temporal d-excess trends. Lowermost d-excess was observed in December 2012 (~8.5) and June/July 2013 (~7.5). Relatively high d-excess was found from late March to early May 2013 (~12). For the complete δD, $\delta^{18}O$, and d-excess time series, the authors refer to Table S2 (online supplement).

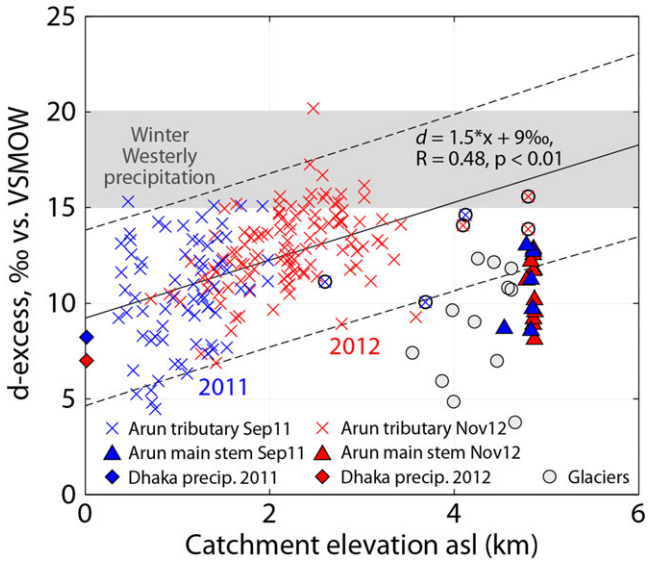

FIGURE 3 d-Excess of main stem (triangles) and tributary (crosses) water samples from 2011 and 2012 colour coded in blue and red, respectively (see Table S1, online supplement for analytical errors). Black circles indicate glaciated tributaries. For comparison, d-excess of Winter Westerly precipitation (Karim & Veizer, 2002; Pande, Padia, Ramesh, & Sharma, 2000) and local glacial melt water d-excess (grey circles, cf. Figure 1a and 1b; Racoviteanu et al., 2013) are shown

4.3 | Rainfall

The temporal analysis of TRMM-recorded rainfall in 2011 and 2012 revealed that 74% and 71% of total annual (January to December) rainfall precipitated during ISM peak season between June and September, respectively. Seven-year mean of catchment-wide cumulative annual rainfall (January–December) during 7 years prior to sampling (2004 to 2010) was on average 982 mm year^{-1} (σ = 127 mm year^{-1}, Figure 5). In 2011, cumulative annual rainfall averaged over the entire Arun catchment was 1,059 mm year^{-1} (35.56 km^3 year^{-1}), and in 2012, it was 881 mm year^{-1} (29.58 km^3 year^{-1}), both within one standard deviation of the 7-year mean. Generally, the lower Arun received more rain than the much larger upper Arun section (Figure 5). Due to its proportionately larger surface area, rainfall volumes in the upper Arun exceeded those in the lower Arun by a factor of roughly three: In 2011, the upper Arun received a total of 944 mm rainfall, being equivalent to a volume of 26.73 km^3 year^{-1}, whereas the lower part received 1,679 mm (8.83 km^3 year^{-1}). In 2012, both parts of the catchment received less rain with 769 mm year^{-1} in the upper Arun (21.78 km^3 year^{-1}, 19% less) and 1,487 mm year^{-1} in the lower Arun (7.82 km^3 year^{-1}, 11% less; Figure 5). We analysed TRMM rainfall in order to account for a seasonal bias due to post-ISM rainfall prior or during the October/November 2012 sampling campaign. The upper Arun received 66 mm of rain in October 2012 and 11 mm in November. During these 2 months, the lower Arun received 57 and 6 mm of rain, making up 3.8% and 0.4% of 2012 cumulative rainfall (1,487 mm), respectively.

The GNIP station in Dhaka, Bangladesh received a total of 1,787 mm of rain in 2011 and 1,316 mm in 2012 with 1,241 and 762 mm during the ISM season from June to September, respectively. Every month in the ISM 2012 season (June–September) received less rain than in 2011 (Figure S4), which is similar to what we observe in the Arun Valley using satellite TRMM rainfall data (Figure 5). This difference is also reflected by ISM seasonal amount weighted mean δD_{precip} with −51.0‰ in 2011 and −31.8‰ in 2012, respectively. The interannual $\Delta D_{2011/2012}$ varied from −6.6‰ in May to −27.5‰ in June with an annual weighted $\Delta D_{2011/2012}$ of −15.3‰ (June–September weighted $\Delta D_{2011/2012}$ = 19.3‰, Figure S4). δD_{precip} in Dhaka is characterized by decreasing δD_{precip} values from the ISM onset until winter with October 2012 δD_{precip} values (−49‰) similar to July and September 2012 δD (−49‰ and −52‰, respectively) and lower November δD_{precip} − 73‰ (Figure S4). The decreasing trend is similar to other observations on temporal δD_{precip} value distribution (Breitenbach et al., 2010, for year 2007; Jeelani, Shah, Jacob, & Deshpande, 2017). However, data by Breitenbach et al. (2010) for 2008 by Yu et al. (2016) indicate an increase of post-ISM δD_{precip}.

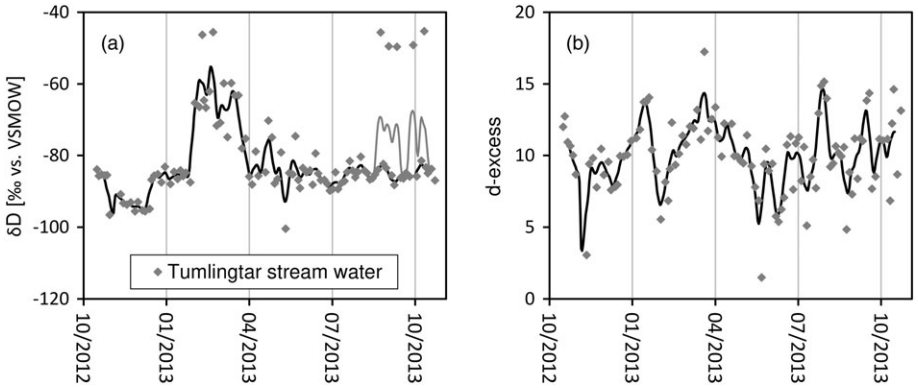

FIGURE 4 (a) Arun river δD value time series from Tumlingtar with Gauss-filtered 15-day running mean including/not including outliers (black line with grey excursion/black line). (b) d-Excess from 11/2012 to 11/2013 at Tumlingtar including Gauss-filtered 15-day running mean. For the data we refer to Table S2, online supplement

4.4 | Snow melt

MODIS snow cover data revealed that the overall snow cover extent in the Arun Valley prior to and during the two field seasons in September 2011 and November 2012 was more or less stable, indicating only little snow melt (Figure 6). The minimum snow cover extent in 2011 and 2012 was reached in the middle of July. The average snow cover of the Arun catchment during the 2011 sampling campaign (2.5%) was on the same order as the 7-year mean (1.9%, 2004–2010). At the beginning of the 2011 sampling campaign, 1.8% of the catchment was covered with snow (lower Arun: 1.8%, upper Arun: 1.8%). During the first 3 weeks, the total snow cover decreased to 0.5% (lower Arun: 0.4%, upper Arun: 0.6%) and increased during the last 6 days of sampling to 5.9% (lower Arun: 3.9%, upper Arun: 6.3%).

During the 2012 sampling campaign, catchment mean snow cover (3.3%) was 3.4% below the 7-year mean of 6.7%. The lower Arun (3.8% in 2012, 5.0% 7-year mean) and the upper Arun (3.2% in 2012, 7.1% 7-year mean) were characterized by similarly small snow cover. At the beginning of the 2012 field season, 4.2% of the Arun catchment was covered with snow (lower Arun: 3.5%, upper Arun: 4.3). Overall snow cover decreased during sampling to 3.1% due to a decrease in the upper Arun (2.9%); in the lower Arun, it remained on the same level (3.5%).

5 | DISCUSSION

Our observations suggest that the isotopic composition of surface water in both sampling years differed significantly, with surface water being more depleted in D in 2011. In the following, we evaluate different hypotheses to explain this observation. First, we consider the effect of WWD derived moisture and evapotranspiration during both years and discuss how they potentially affect surface water δD values. Subsequently, we evaluate the effect of glacial melt contribution on the Arun Valleys' surface water. Last, we discuss to what extent the observed $\Delta D_{2011/2012}$ may have been driven by variable ISM and assess the consequences for the reconstruction of ISM $\delta D/\delta^{18}O$ values in the eastern central Himalaya based on stable isotope archives.

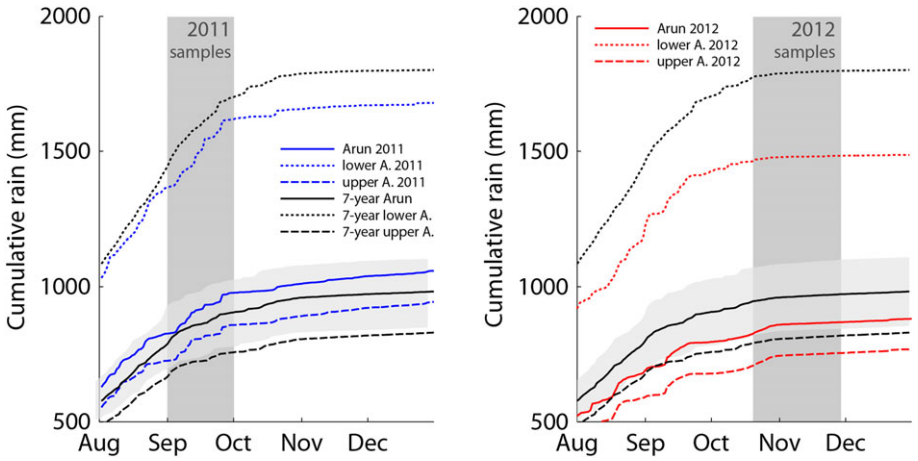

FIGURE 5 TRMM V3B42 (Bookhagen, 2010) derived Jan–Dec cumulative rain during 2011 (left, blue lines) and 2012 (right, red lines) sampling campaigns in comparison with 7-year mean cumulative rainfall (2004–2010, black lines). For better visualization of spatial rainfall variability, we show the average cumulative rain of the entire Arun catchment (solid lines), cumulative rain in the lower Arun (dotted lines), and in the upper Arun (dashed lines). Shaded boxes denote sampling periods. X-axis ticks denote the beginning of each month

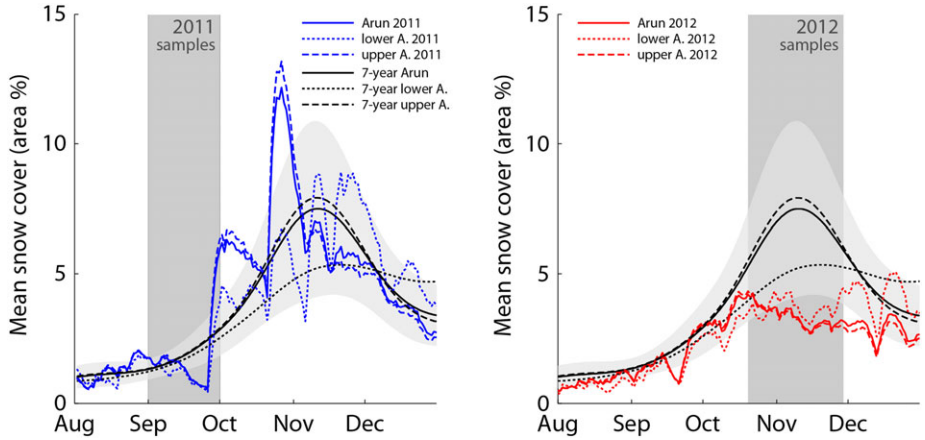

FIGURE 6 Daily snow-cover extent in 2011 (left, blue lines) and 2012 (right, red lines) in comparison with the 7-year mean (2004–2010, black lines). Boxes indicate the timing of sampling campaigns. Mean snow cover in 2011 across the entire catchment was within the range of the 7-year mean. In 2012, especially the upper Arun exhibits a lower snow cover compared with the 7-year mean. During both sampling campaigns, overall snow cover decreased by less than 1.1%, indicating very low melt water release

5.1 | Winter Westerlies and snow melt

In addition to the ISM, WWD result in D-depleted precipitation serving as water source for the high altitude part of the Arun catchment (Cannon et al., 2015; Hren et al., 2009; Karim & Veizer, 2002; Lang & Barros, 2004). However, most streams sampled in September 2011 that were characterized by comparably D-depleted water were located at low elevations, which hardly receive WWD moisture and snow, opposed to most streams sampled in 2012. Hence, stronger D-depletion of surface water sampled in 2011 could not have been caused by an enhanced melt of Winter-Westerly derived snow. This argument is supported by remotely sensed snow cover, the timing of Winter Westerlies, and surface water d-excess data: MODIS snow cover analysis revealed similar negligible snow cover decline before and during both field seasons, suggesting only minor snow meltwater contributions in September 2011 and November 2012 (Figure 6). This is backed by the timing of WWD, which occur predominantly between January and March (Lang & Barros, 2004), implying a potential effect on stream waters months after the sampling campaign of either year. An increased contribution of WWD snow with a d-excess of approximately 15–20‰ (Karim & Veizer, 2002; Pande et al., 2000) would necessarily result in lower surface water δD values and increased d-excess, which contradicts our observations (Figures 2a and 3). The time series data (Figure 4) indicate the largest snow melt fraction of Arun main stem waters in April, where δD values drop after winter but d-excess remains on a comparably high level. This corresponds well to other studies reporting major snow melt impact in spring as direct surface run-off (Smith et al., 2017) and protracted run-off during the ISM onset in May to June after temporal storage in the vadose zone (Buttle, 1994).

The observed increase d-excess with altitude until ~3 km asl observed in 2011 and 2012 (Figure 3) is typical for Rayleigh type rain out at mountain fronts (Gonfiantini et al., 2001; Xu et al., 2014). Above ~3 km, tributary and main stem d-excess did not increase anymore, interpreted as increased fraction of reworked water in high-altitude precipitation (Karim & Veizer, 2002; Pande et al., 2000). On the basis of our observations on September 2011 and October/November 2012 d-excess and the time series data from Tumlingtar, we argue that snowmelt had similar minor effects on sampled surface water δD values in September 2011 and November 2012 and does not coincide with either sampling campaign. Hence, snowmelt contribution did not cause observed isotopic differences.

5.2 | Evaporative effects

Theoretically, deuterium-enriched surface water in 2012 could be related to increased surface and soil water evaporation. However, remotely sensed evapotranspiration within the Arun catchment indicate similar conditions in 2011 and 2012 (cf. section S2 and Figure S2). The 2011 and 2012 $\delta^{18}O_{sw}/\delta D_{sw}$ regression slopes (Table 2) are similar and comparable with data from an Arun tributary sampled by Balestrini, Polesello, and Sacchi (2014) in fall 2007 (Khumbu Valley, $\delta D = \delta^{18}O$ *7.48 (±0.44) + 2.71 (±7.53‰)), supporting the statement above. Evaporative-water loss required to cause observed D-enrichment in 2012 would necessarily lead to substantially different d-excess for both years (e.g., Gibson, Edwards, & Bursey, 1993). But as discussed in the previous section, we relate the observed pattern to Rayleigh fractionation at plateau margins below 3 km asl (e.g., Gonfiantini et al., 2001; Rowley et al., 2001; Xu et al., 2014) and an increased fraction of reworked water in precipitation above (Karim & Veizer, 2002; Pande et al., 2000). The increasing fraction of reworked water in fall is also reflected by Arun main stem time series data, due to the input of progressively lighter precipitation d-excess decreased until December 2012. We thus argue that evaporative D-enrichment was at a low level prior to and during either sampling campaign and had a considerable effect on tributaries above 3 km only. Interannual evaporation variability, however, can therefore be neglected as underlying cause for observed $\Delta D_{2011/2012}$.

5.3 | Glacial melt

As the offset between 2011 and 2012 δD_{sw} values was observed for main stem and tributary waters with and without glaciated catchments, variable glacial melt water contributions cannot explain

$\Delta D_{2011/2012}$ for all sampled streams. However, melt water contributions of ablating glaciers along the main Himalayan crest (Bolch et al., 2012; Scherler, Bookhagen, & Strecker, 2011) significantly affect the water balance of high altitude catchments (Racoviteanu et al., 2013; Wilson et al., 2016), and in particular, the Arun main stem. The Dudh Kosi and Trishuli watersheds within and west of the Arun catchment, respectively (Figure 1a and 1b), were characterized by a mean δD of −106.3‰ (σ = 11.6‰, n = 12) with a d-excess of 9.0‰ (σ = 2.9‰), when limited to glacier-mouth samples only (Racoviteanu et al., 2013). Average $\delta^{18}O$ values of ice accumulated between 1813 and 1997 in the Dasuopu and East Rongbuk Glaciers 125 and 50 km west of the Arun, respectively, was −17 and −19‰ (Pang, Hou, Kaspari, & Mayewski, 2014). These amounts are equivalent to δD values of −122 and −138‰ when converted with the local meteoric waterline by Yu et al. (2016; Tingri station). Arun main stem δD_{sw} values and those of glaciated tributaries fall in between isotopically heavy tributary water dominated by the ISM and glacial melt water (Pang et al., 2014; Racoviteanu et al., 2013; Figure 2a). As such, a mixture of both water pools in Arun main stem water and the five glaciated tributaries is conceivable. Observed d-excess of respective water samples also correspond well to that of glacial melt (Racoviteanu et al., 2013) and reinforce the argument for strong glacial melt mixing as no other water source has the potential to generate observed low main stem and glaciated tributary d-excess on the southern Tibetan Plateau (Figure 3). The finding of strong glacial melt input mixed with ISM derived rainfall in Arun main stem water and its glaciated tributaries is in agreement with previous findings from the eastern central Himalaya (Racoviteanu et al., 2013; Wilson et al., 2016). However, Arun main stem δD_{sw} values in September 2011 were lower than in November 2012 (Figure 2a), which can be interpreted as a larger contribution of glacial melt in 2011. But similar d-excess in 2011 and 2012 are inconsistent with this interpretation, as they indicate a comparable fraction of glacial melt in both years' main stem water. Hence, variable glacial melt contribution cannot provide a reasonable explanation for the observed main stem and tributary $\Delta D_{2011/2012}$.

5.4 | ISM effects on surface water δD values

ISM-derived precipitation is the major water source in the eastern Nepalese Himalaya (Bookhagen & Burbank, 2010) with 71% and 74% of annual (Jan–Dec) precipitation in 2011 and 2012, respectively. Thus, isotopic lapse rates of −9.56 ± 1.08‰ km^{-1} and −8.24 ± 0.65‰ km^{-1} in September 2011 and November 2012 reflect Rayleigh fractionation effects due to rain out and decreasing temperature (Dansgaard, 1964) across orographic barriers. This effect, often referred to as the altitude effect, is well known and has been observed across major orographic ranges (Rohrmann et al., 2014; Rowley & Garzione, 2007; Xu et al., 2014). The observed Arun Valley isotope lapse rates are comparable with previous studies from the eastern and central Himalaya (Garzione et al., 2000; Hren et al., 2009; Xu et al., 2014) when considering a similar altitudinal range. The linear correlation of both years' d-excess with respect to catchment altitude also reflects rainout at orographic barriers (Hren et al., 2009; Rowley & Garzione, 2007). Whereas both years' separate datasets do not cover an altitude range large enough for a significant correlation, the combined 2011 and 2012 data indicate similar fractionation processes below a mean catchment elevation of 3 km asl emphasizing the ISM predominance in the Arun Valley.

Isotope data from the ISM dominated Dhaka GNIP station in Bangladesh, located on the ISM path just after water vapour leaves the Bay of Bengal and heading north to the Himalaya (Figure 1), show a similar interannual pattern compared with the Arun catchment. 2011 cumulative ISM rainfall (JJAS) in Dhaka was larger (1,241 mm) and the weighted mean δD_{precip} value (−51.0‰) lower than in 2012 (JJAS, 762 mm, −31.8‰). This is consistent with the amount effect, that is, lower δD_{precip} values at higher precipitation amounts, as often observed in the tropics (Kurita et al., 2009), although regional δD_{precip} values are controlled by additional factors (Breitenbach et al., 2010). The 2012 IMI was 1.95 standard deviations below the 1948–2013 average, whereas it was close to the 65-year mean in 2011 (−0.56), pointing towards a particularly weak monsoon in 2012 compared with 2011. The weaker 2012 ISM with less rainfall in the Arun Valley is also supported by satellite-derived TRMM cumulative rainfall rates: 2012 ISM rainfall in the lower Arun was 17% lower compared with 2011. This observation strongly suggests that the variable ISM isotopic signature observed in Dhaka is carried onwards to the Himalaya where it is manifested in δD_{precip} values along the orographic front. However, sampling in 2011 was conducted during late ISM (September), whereas samples in 2012 were collected in the post-ISM season (October and November). TRMM-derived rainfall rates for October/November 2012 in the Arun Valley were 57 and 6 mm, respectively. Hence, there was a small volume of post-ISM rainfall that might have affected sampled surface waters in 2012. Reported data of post-ISM rainfall δD_{precip} are variable with both, increasing and decreasing δD_{precip} values (Breitenbach et al., 2010; Jeelani et al., 2017; Karim & Veizer, 2002; Yu et al., 2016). Tumlingtar time series δD_{sw} values decrease until the end of December, suggesting that post-ISM δD_{precip} values were below ISM δD_{precip}, similar to observations from Dhaka (Figure S4). Hence, post-ISM rainfall would have reduced 2012 surface water δD values and therefore $\Delta D_{2011/2012}$. However, the amount of October/November rain in the lower Arun in 2012 made up 4.2% of cumulative annual precipitation in 2012. Considering this relative rainfall volume, the altering effect of post-ISM rainfall on $\Delta D_{2011/2012}$ is assumed to be fairly small. In spite of the potential minor effect of seasonality on $\Delta D_{2011/2012}$, the analysis of stationary precipitation, IMI, and remote sensing rainfall data indicates that $\Delta D_{2011/2012}$ in the Arun Valley was a consequence of interannual ISM variability.

5.5 | Implications for palaeoclimate applications

Our analysis revealed that the interannual ISM strength variability in 2011 and 2012 was reflected by surface water δD values of both tributary and main stem waters. Although surface water represent a complex mixture of surface run-off, ground-water fed base flow, and other potential water sources, such as glacial and snow melt (Andermann et al., 2012; Oshun, Dietrich, Dawson, & Fung, 2016; Racoviteanu et al., 2013; Smith et al., 2017; Wilson et al., 2016), our results imply that the Arun Valley and especially its southern tributaries are very sensitive to ISM δD values. The observation of surface water δD

values reflecting interannual variable ISM trajectories and amount has an important consequence for the temporal resolution of potential stable isotope records being used for palaeohydrology: Changes of δD_{precip} values in the Arun Valley due to ISM variability may theoretically be recorded annually and are rather limited by temporal recording capacities of the proxy.

Our data from the Arun Valley suggest that δD_{sw} values of tributaries, spatially integrating over catchments ranging from 10^{-1} to 10^2 km^2, reflect ISM δD_{precip} values. The spatial integration capacity of tributaries is an important aspect concerning, for example, lacustrine biomarker records and speleothems in this region. As such, palaeorecords below the snowline integrate δD_{precip} values on similar or smaller spatial scales as analysed tributaries. Hence, such archives are suitable for past ISM δD_{precip} value reconstruction and can potentially serve as quantitative ISM proxy. However, the non-linear relationship of ISM strength and δD_{precip} at the Dhaka GNIP station indicates that δD_{precip} only partly reflects ISM strength (Figure S4). This is in agreement with Breitenbach et al. (2010), who found moisture transport distance and Bay of Bengal surface water isotope composition to have major controls on δD_{precip} values at the southern front of the Shillong Plateau (Figure 1a). Hence, setting up a robust calibration function capable of converting δD_{sw} palaeovalues into ISM strength requires a longer time series of surface water stable isotopic composition and additional remote sensing climate data.

The interpretation of stable hydrogen and oxygen isotope archives in the upper Arun Valley and its high altitude catchments is even more complex as they yield mixed signals of WWD precipitation, ISM rainfall, and glacial melt. The same applies to the interpretation of fluvial archives along the Arun main stem (Hoffmann et al., 2016). First, fluvial archives are likely affected by WWD precipitation in the high-elevation parts of the catchment, although it had no effect on sampled main stem water due to the timing of sampling several months prior to snow melt. Second and more importantly, the Arun is affected by glacial melt; its signal is persistent all along the river, even at the southernmost sample site at the Nepalese–Indian border (sample 11104, Koshi Barrage Bridge). But because tributaries south of the Himalayan crest below the snow line predominantly receive ISM-derived summer precipitation, we note the high potential of stable isotope archives in that region for qualitative and potentially quantitative palaeo-ISM reconstruction.

6 | CONCLUSION

In order to understand the influence of the ISM on water δD and $\delta^{18}O$ values in the eastern central Himalaya, we followed an approach combining stable isotope measurements and remote sensing data analysis: We first determined δD and $\delta^{18}O$ values of the eastern Nepalese Arun River and its tributary water sampled in fall 2011 and 2012. Additionally, we recorded Arun main stem surface water δD and $\delta^{18}O$ for one annual cycle in order to determine seasonal variability of different moisture sources. Second, we analysed satellite remote sensing data of rainfall, snow cover, glacial coverage, and evapotranspiration related to both sampling campaigns. These data show important observation crucial to the interpretation of present and past ISM changes.

Our study revealed three key findings: First, we found the 2012 ISM to be significantly weaker than the 2011 ISM with ~20% less June to September rainfall in the Arun Valley. As a consequence, main stem and tributary surface water δD values in 2012 were enriched by ~15‰ compared with the previous year, emphasizing the sensitivity of the Arun Valley hydrology to ISM variability. Second, δD and d-excess value distributions indicate that high-altitude tributary catchments and the Tibetan Plateau received large volumes of glacial melt in addition to the evident ISM contribution across the entire Arun Valley. Third, remote sensing snow cover data indicated that high-altitude tributaries and the Tibetan Plateau part north of the Nepalese–Chinese border receive winter precipitation, presumably derived from WWD. In the Arun time series, the isotopic signature of snow melt was observed between March and May. Although it could not be quantified to which extent the Arun Valley hydrology is affected by snow melt, we show that it did not affected September 2011 and November 2012 surface water samples. In order to better determine the effect of variable ISM strength and to quantify snow and glacial melt, a long-term time series of Arun main stem and tributary δD_{sw} is required.

Our data from the Arun Valley tributaries indicate that stable isotope proxy records from south of the eastern central Himalayan crest are well suited to reconstruct past ISM δD values and by extension ISM strength—although we caution that this relationship is likely non-linear. First, tributaries respond quickly to water input from isotopically distinct reservoirs, and second, they integrate the isotopic composition of precipitation on similar spatial scales as potential stable isotope proxy records and clearly reflect ISM δD and $\delta^{18}O$ values.

ACKNOWLEDGMENTS

B. H. was funded through DFG GRK 1364 and D. S. through an Emmy-Noether grant from the German Science Foundation (DFG SA1889/1-1 and 1-2). Thanks to Danda P. Adhikari for logistical support, Janardan Mainali, Manoj, Sophia Wagner, Raphael Scheffler, and Michael Pöhle for field and lab assistance.

ORCID

Bernd Meese http://orcid.org/0000-0002-1413-8321
Bodo Bookhagen http://orcid.org/0000-0003-1323-6453
Dirk Sachse http://orcid.org/0000-0003-4207-0309

REFERENCES

Andermann, C., Longuevergne, L., Bonnet, S., Crave, A., Davy, P., & Gloaguen, R. (2012). Impact of transient groundwater storage on the discharge of Himalayan rivers. *Nature Geoscience*, *5*(2), 127–132. https://doi.org/10.1038/ngeo1356

Araguás Araguás, L., & Froehlich, K. (1998). Stable isotope composition of precipitation over southeast Asia. *Journal of Geophysical Research*, *103*(D22), 28721–28742. https://doi.org/10.1029/98JD02582/full

Balestrini, R., Polesello, S., & Sacchi, E. (2014). Chemistry and isotopic composition of precipitation and surface waters in Khumbu valley (Nepal Himalaya): N dynamics of high elevation basins. *Science of the Total Environment*, *485–486*(1), 681–692. https://doi.org/10.1016/j.scitotenv.2014.03.096

Berkelhammer, M., Sinha, A., Mudelsee, M., Cheng, H., Edwards, R. L., & Cannariato, K. (2010). Persistent multidecadal power of the Indian

Summer Monsoon. *Earth and Planetary Science Letters*, *290*(1–2), 166–172. https://doi.org/10.1016/j.epsl.2009.12.017

Blisniuk, P. M., & Stern, L. a. (2005). Stable isotope paleoaltimetry: A critical review. *American Journal of Science*, *305*(10), 1033–1074. https://doi.org/10.2475/ajs.305.10.1033

Bolch, T., Kulkarni, a., Kaab, a., Huggel, C., Paul, F., Cogley, J. G., et al. (2012). The state and fate of Himalayan glaciers. *Science*, *336*(6079), 310–314. https://doi.org/10.1126/science.1215828

Bookhagen B. 2010. TRMM V4 Available at: http://www.geog.ucsb.edu/$~$bodo/pdf/bookhagen10_extreme_rainfall_Himalaya.pdf

Bookhagen, B., & Burbank, D. W. (2006). Topography, relief, and TRMM-derived rainfall variations along the Himalaya. *Geophysical Research Letters*, *33*(8), L08405. https://doi.org/10.1029/2006GL026037

Bookhagen, B., & Burbank, D. W. (2010). Toward a complete Himalayan hydrological budget: Spatiotemporal distribution of snowmelt and rainfall and their impact on river discharge. *Journal of Geophysical Research*, *115*(F3), F03019. https://doi.org/10.1029/2009JF001426

Breitenbach, S. F. M., Adkins, J. F., Meyer, H., Marwan, N., Kumar, K. K., & Haug, G. H. (2010). Strong influence of water vapor source dynamics on stable isotopes in precipitation observed in Southern Meghalaya, NE India. *Earth and Planetary Science Letters*, *292*(1–2), 212–220. https://doi.org/10.1016/j.epsl.2010.01.038

Buttle, J. M. (1994). Isotope hydrograph separations and rapid delivery of pre-event water from drainage basins. *Progress in Physical Geography*, *18*(1), 16–41. https://doi.org/10.1177/030913339401800102

Cannon, F., Carvalho, L. M. V., Jones, C., & Bookhagen, B. (2015). Multi-annual variations in winter westerly disturbance activity affecting the himalaya. *Climate Dynamics*, *44*(1–2), 441–455. https://doi.org/10.1007/s00382-014-2248-8

Dansgaard, W. (1964). Stable isotopes in precipitation. *Tellus*, *16*(4), 436–468. https://doi.org/10.3402/tellusa.v16i4.8993

Dansgaard, W., Clausen, H. B., Gundestrup, N., Hammer, C. U., Johnsen, S. F., Kristinsdottir, P. M., & Reeh, N. (1982). A new Greenland deep ice core. *Science*, *218*(4579), 1273–1277.

DeWalle, D., Edwards, P., Swistock, B., Aravena, R., & Drimmie, R. (1997). Seasonal isotope hydrology of three Appalachian forest catchments. *Hydrological Processes*, *11*, 1895–1906. https://doi.org/10.1002/(SICI)1099-1085(199712)11:15<1895::AID-HYP538>3.3.CO;2-R

Freeman, K. H., & Colarusso, L. A. (2001). Molecular and isotopic records of C4 grassland expansion in the late miocene. *Geochimica et Cosmochimica Acta*, *65*(9), 1439–1454. https://doi.org/10.1016/S0016-7037(00)00573-1

Garzione, C. N., Quade, J., DeCelles, P. G., & English, N. B. (2000). Predicting paleoelevation of Tibet and the Himalaya from $\delta^{18}O$ vs. altitude gradients in meteoric water across the Nepal Himalaya. *Earth and Planetary Science Letters*, *183*(1–2), 215–229. https://doi.org/10.1016/S0012-821X(00)00252-1

Gibson, J. J., Edwards, T. W. D., & Bursey, G. G. (1993). Estimating Evaporation Using Stable Isotopes: Quantitative Results and Sensitivity Analysis for Two Catchments in Northern Canada. *Nordic Hydrology*, *24*(2–3), 79–94. https://doi.org/10.2166/nh.1993.006

Gonfiantini, R., Roche, M.-A., Olivry, J.-C., Fontes, J.-C., & Zuppi, G. M. (2001). The altitude effect on the isotopic composition of tropical rains. *Chemical Geology*, *181*(1–4), 147–167. https://doi.org/10.1016/S0009-2541(01)00279-0

Hall, D. K., Riggs, G. A., Salomonson, V. V., DiGirolamo, N. E., & Bayr, K. J. (2002). MODIS snow-cover products. *Remote Sensing of Environment*, *83*(1–2), 181–194. https://doi.org/10.1016/S0034-4257(02)00095-0

Hendy, C. H. (1971). The isotopic geochemistry of speleothems-I. The calculation of the effects of different modes of formation on the isotopic composition of speleothems and their applicability as palaeoclimatic indicators. *Geochimica et Cosmochimica Acta*, *35*(8), 801–824. https://doi.org/10.1016/0016-7037(71)90127-X

Hendy, C. H., & Wilson, a. T. (1968). Palaeoclimatic data from speleothems. *Nature*, *219*(5149), 48–51. https://doi.org/10.1038/219048a0

Hoffmann, B., Feakins, S. J., Bookhagen, B., Olen, S. M., Adhikari, D. P., Mainali, J., & Sachse, D. (2016). Climatic and geomorphic drivers of plant organic matter transport in the Arun River, E Nepal. *Earth and Planetary Science Letters*, *452*, 104–114. https://doi.org/10.1016/j.epsl.2016.07.008

Hren, M. T., Bookhagen, B., Blisniuk, P. M., Booth, A. L., & Chamberlain, C. P. (2009). delta O-18 and delta D of streamwaters across the Himalaya and Tibetan Plateau: Implications for moisture sources and paleoelevation reconstructions. *Earth and Planetary Science Letters*, *288*(1–2), 20–32. https://doi.org/10.1016/j.epsl.2009.08.041

Huang, Y., Shuman, B., Wang, Y., & Webb, T. (2004). Hydrogen isotope ratios of individual lipids in lake sediments as novel tracers of climatic and environmental change: A surface sediment test. *Journal of Paleolimnology*, *31*(3), 363–375. https://doi.org/10.1023/B:JOPL.0000021855.80535.13

Huffman, G. J., Bolvin, D. T., Nelkin, E. J., Wolff, D. B., Adler, R. F., Gu, G., … Stocker, E. F. (2007). The TRMM multisatellite precipitation analysis (TMPA): Quasi-global, multiyear, combined-sensor precipitation estimates at fine scales. *Journal of Hydrometeorology*, *8*(1), 38–55. https://doi.org/10.1175/JHM560.1

Jarvis A, Reuter HI, Nelson A. 2008. Hole-filled SRTM for the globe Version 4, available from the CGIAR-CSI SRTM 90m Database (http://srtm.csi.cgiar.org).

Jeelani, G., Shah, R. A., Jacob, N., & Deshpande, R. D. (2017). Estimation of snow and glacier melt contribution to Liddar stream in a mountainous catchment, western Himalaya: An isotopic approach. *Isotopes in Environmental and Health Studies*, *53*(1), 18–35. https://doi.org/10.1080/10256016.2016.1186671

Johnsen, S., Dahl-jensen, D., Dansgaard, W., & Gundestrup, N. S. (1995). Greenland palaeotemperatures derived from GRIP bore hole temperature and ice core isotope profiles. *Tellus*, *47B*, 624–629. https://doi.org/10.1034/j.1600-0889.47.issue5.9.x

Karim, A., & Veizer, J. (2002). Water balance of the Indus River Basin and moisture source in the Karakoram and western Himalayas: Implications from hydrogen and oxygen isotopes in river water. *Journal of Geophysical Research: Atmospheres*, *107*, 1–12. https://doi.org/10.1029/2000JD000253

Kotlia, B. S., Ahmad, S. M., Zhao, J. X., Raza, W., Collerson, K. D., Joshi, L. M., & Sanwal, J. (2012). Climatic fluctuations during the LIA and post-LIA in the Kumaun Lesser Himalaya, India: Evidence from a 400 y old stalagmite record. *Quaternary International*, *263*, 129–138. https://doi.org/10.1016/j.quaint.2012.01.025

Kotlia, B. S., Singh, A. K., Joshi, L. M., & Dhaila, B. S. (2015). Precipitation variability in the Indian Central Himalaya during last ca. 4,000 years inferred from a speleothem record: Impact of Indian Summer Monsoon (ISM) and Westerlies. *Quaternary International*, *371*, 244–253. https://doi.org/10.1016/j.quaint.2014.10.066

Kurita, N., Ichiyanagi, K., Matsumoto, J., Yamanaka, M. D., & Ohata, T. (2009). The relationship between the isotopic content of precipitation and the precipitation amount in tropical regions. *Journal of Geochemical Exploration*, *102*(3), 113–122. https://doi.org/10.1016/j.gexplo.2009.03.002

Lang, T. J., & Barros, A. P. (2004). Winter storms in the central Himalayas. *Journal of the Meteorological Society of Japan*, *82*(3), 829–844. https://doi.org/10.2151/jmsj.2004.829

Lekshmy, P. R., Midhun, M., Ramesh, R., & Jani, R. A. (2014). ^{18}O depletion in monsoon rain relates to large scale organized convection rather than the amount of rainfall. *Scientific Reports*, *4*(5661), 1–5. https://doi.org/10.1038/srep05661

Li, Y., Wang, N., Zhou, X., Zhang, C., & Wang, Y. (2014). Synchronous or asynchronous Holocene Indian and East Asian summer monsoon evolution: A synthesis on Holocene Asian summer monsoon simulations, records and modern monsoon indices. *Global and Planetary Change*, *116*, 30–40. https://doi.org/10.1016/j.gloplacha.2014.02.005

Liang, F., Brook, G. A., Kotlia, B. S., Railsback, L. B., Hardt, B., Cheng, H., … Kandasamy, S. (2015). Panigarh cave stalagmite evidence of climate change in the Indian Central Himalaya since AD 1256: Monsoon breaks and winter southern jet depressions. *Quaternary Science Reviews*,

124(SEPTEMBER), 145–161. https://doi.org/10.1016/j.quascirev.2015.07.017

Lister, G. S., Kelts, K., Zao, C. K., Yu, J.-Q., & Niessen, F. (1991). Lake Qinghai, China: Closed-basin like levels and the oxygen isotope record for ostracoda since the latest Pleistocene. *Palaeogeography, Palaeoclimatology, Palaeoecology*, *84*(1–4), 141–162. https://doi.org/10.1016/0031-0182(91)90041-O

Liu, Z., Henderson, A. C. G., & Huang, Y. (2008). Regional moisture source changes inferred from Late Holocene stable isotope records. *Advances in Atmospheric Sciences*, *25*(6), 1021–1028. https://doi.org/10.1007/s00376-008-1021-5

Malik, N., Bookhagen, B., & Mucha, P. J. (2016). Spatiotemporal patterns and trends of Indian monsoonal rainfall extremes. *Geophysical Research Letters*, 1–22. https://doi.org/10.1002/2016GL067841

Mooley, D. A., & Parthasarathy, B. (1984). Fluctuations in All-India summer monsoon rainfall during 1871-1978. *Climatic Change*, *6*(3), 287–301. https://doi.org/10.1007/BF00142477

Mu, Q., Zhao, M., & Running, S. W. (2011). Improvements to a MODIS global terrestrial evapotranspiration algorithm. *Remote Sensing of Environment*, *115*(8), 1781–1800. https://doi.org/10.1016/j.rse.2011.02.019

Olen, S. M., Bookhagen, B., Hoffmann, B., Sachse, D., Adhikari, D. P., & Strecker, M. R. (2015). Understanding erosion rates in the Himalayan orogen: A case study from the Arun Valley. *Journal of Geophysical Research: Earth Surface*, *120*, 2080–2102. https://doi.org/10.1002/2014JF003410

Oshun, J., Dietrich, W. E., Dawson, T. E., & Fung, I. (2016). Dynamic, structured heterogeneity of water isotopes inside hillslopes. *Water Resources Research*, *52*(1), 164–189. https://doi.org/10.1002/2015WR017485

Pande, K., Padia, J. T., Ramesh, R., & Sharma, K. K. (2000). Stable isotope systematics of surface water bodies in the Himalayan and Trans-Himalayan (Kashmir) region. *Proc. Indian Acad. Sci. (Earth Planet. Sci.)*, *109*(1), 109–115. https://doi.org/10.1007/bf02719154

Pang, H., Hou, S., Kaspari, S., & Mayewski, P. A. (2014). Influence of regional precipitation patterns on stable isotopes in ice cores from the central Himalayas. *The Cryosphere*, *8*(1), 289–301. https://doi.org/10.5194/tc-8-289-2014

Parthasarathy, B., Rupa Kumar, K., & Kothawale, D. R. (1992). Indian summer monsoon rainfall indices: 1871-1990. *Meteorological Magazine*, *121*(1441), 174–186.

Ponton, C., Giosan, L., Eglinton, T. I., Fuller, D. Q., Johnson, J. E., Kumar, P., & Collett, T. S. (2012). Holocene aridification of India. *Geophysical Research Letters*, *39*(3), 1–6. https://doi.org/10.1029/2011GL050722

Racoviteanu, A. E., Armstrong, R., & Williams, M. W. (2013). Evaluation of an ice ablation model to estimate the contribution of melting glacier ice to annual discharge in the Nepal Himalaya. *Water Resources Research*, *49*(January), 5117–5133. https://doi.org/10.1002/wrcr.20370

Rohrmann, A., Strecker, M. R., Bookhagen, B., Mulch, A., Sachse, D., Pingel, H., … Montero, C. (2014). Can stable isotopes ride out the storms? The role of convection for water isotopes in models, records, and paleoaltimetry studies in the central Andes. *Earth and Planetary Science Letters*, *407*, 187–195. https://doi.org/10.1016/j.epsl.2014.09.021

Rowley, D. B., & Garzione, C. N. (2007). Stable isotope-based paleoaltimetry. *Annual Review of Earth and Planetary Sciences*, *35*(1), 463–508. https://doi.org/10.1146/annurev.earth.35.031306.140155

Rowley, D. B., Pierrehumbert, R. T., & Currie, B. S. (2001). A new approach to stable isotope-based paleoaltimetry: implications for paleoaltimetra and paleohypsometry of the High Himalaya since the Late Miocene. *Earth and Planetary Science Letters*, *5836*(2001), 1–17.

Rozanski, K., Araguás-Araguás, L., & Gonfiantini, R. (1993). Isotopic patterns in modern global precipitation. *Climate Change in Continental Isotopic Records*, (JANUARY), 1–36. https://doi.org/10.1029/GM078p0001

Sachse, D., Radke, J., & Gleixner, G. (2004). Hydrogen isotope ratios of recent lacustrine sedimentary n-alkanes record modern climate variability. *Geochimica et Cosmochimica Acta*, *68*(23), 4877–4889. https://doi.org/10.1016/j.gca.2004.06.004

Sanwal, J., Kotlia, B. S., Rajendran, C., Ahmad, S. M., Rajendran, K., & Sandiford, M. (2013). Climatic variability in Central Indian Himalaya during the last ~1800 years: Evidence from a high resolution speleothem record. *Quaternary International*, *304*, 183–192. https://doi.org/10.1016/j.quaint.2013.03.029

Sarkar, S., Prasad, S., Wilkes, H., Riedel, N., Stebich, M., Basavaiah, N., & Sachse, D. (2015). Monsoon source shifts during the drying mid-Holocene: Biomarker isotope based evidence from the core 'monsoon zone' (CMZ) of India. *Quaternary Science Reviews*, *123*(December), 144–157. https://doi.org/10.1016/j.quascirev.2015.06.020

Schefuß, E., Ratmeyer, V., Stuut, J.-B. W., Jansen, J. H. F., & Sinninghe Damsté, J. S. (2003). Carbon isotope analyses of n-alkanes in dust from the lower atmosphere over the central eastern Atlantic. *Geochimica et Cosmochimica Acta*, *67*(10), 1757–1767. https://doi.org/10.1016/S0016-7037(02)01414-X

Scherler, D., Bookhagen, B., & Strecker, M. R. (2011). Spatially variable response of Himalayan glaciers to climate change affected by debris cover. *Nature Geoscience*, *4*(3), 156–159. https://doi.org/10.1038/ngeo1068

Sinha, A., Berkelhammer, M., Stott, L., Mudelsee, M., Cheng, H., & Biswas, J. (2011). The leading mode of Indian Summer Monsoon precipitation variability during the last millennium. *Geophysical Research Letters*, *38*(15), 2–6. https://doi.org/10.1029/2011GL047713

Sinha, A., Cannariato, K. G., Stott, L. D., Cheng, H., Edwards, R. L., Yadava, M. G., … Singh, I. B. (2007). A 900-year (600 to 1500 A.D.) record of the Indian summer monsoon precipitation from the core monsoon zone of India. *Geophysical Research Letters*, *34*(16), 1–5. https://doi.org/10.1029/2007GL030431

Sinha, A., Cannariato, K. G., Stott, L. D., Li, H.-C., You, C.-F., Cheng, H., … Singh, I. B. (2005). Variability of Southwest Indian summer monsoon precipitation during the Bølling-Ållerød. *Geology*, *33*(10), 813. https://doi.org/10.1130/G21498.1

Smith, T., Bookhagen, B., & Rheinwalt, A. (2017). Spatiotemporal patterns of High Mountain Asia's snowmelt season identified with an automated snowmelt detection algorithm, 1987–2016. *The Cryosphere*, *11*(5), 2329–2343. https://doi.org/10.5194/tc-11-2329-2017

Soulsby, C., Malcolm, R., Helliwell, R., Ferrier, R. C., & Jenkins, A. (2000). Isotope hydrology of the Allt a'Mharcaidh catchment, Cairngorms, Scotland: Implications for hydrological pathways and residence times. *Hydrological Processes*, *14*(4), 747–762. https://doi.org/10.1002/(SICI)1099-1085(200003)14:4<747::AID-HYP970>3.0.CO;2-0

Tedesco M, Kelly R, Foster JLL, Chang ATCTC. 2004. AMSR-E/Aqua Daily L3 Global Snow Water Equivalent EASE-Grids, Version 2. DOI: https://doi.org/10.5067/AMSR-E/AE{_}DYSNO.002

Thompson, L. G., Yao, T., Mosley-Thompson, E., Davis, M. E., Henderson, K. A., & Lin, P. N. (2000). A high-resolution millennial record of the South Asian Monsoon from Himalayan ice cores. *Science*, *289*(5486), 1916–1919. https://doi.org/10.1126/science.289.5486.1916

Tian, L., Yao, T., Schuster, P. F., White, J. W. C., Ichiyanagi, K., Pendall, E., … Yu, W. (2003). Oxygen-18 concentrations in recent precipitation and ice cores on the Tibetan Plateau. *Journal of Geophysical Research*, *108*(D9), 1–10. https://doi.org/10.1029/2002JD002173

Tierney, J. E., Russell, J. M., Huang, Y., Damste, J. S. S., Hopmans, E. C., & Cohen, A. S. (2008). Northern hemisphere controls on tropical southeast African climate during the past 60,000 years. *Science*, *322*(5899), 252–255. https://doi.org/10.1126/science.1160485

Wang, B., & Fan, Z. (1999). Choice of South Asian summer monsoon indices. *Bulletin of the American Meteorological Society*, *80*(4), 629–638. https://doi.org/10.1175/1520-0477(1999)080<0629:COSASM>2.0.CO;2

Wilson, A. M., Williams, M. W., Kayastha, R. B., & Racoviteanu, A. (2016). Use of a hydrologic mixing model to examine the roles of meltwater, precipitation and groundwater in the Langtang River basin, Nepal. *Annals of Glaciology*, *57*(71), 155–168. https://doi.org/10.3189/2016AoG71A067

Wulf, H., Bookhagen, B., & Scherler, D. (2016). Differentiating between rain, snow, and glacier contributions to river discharge in the western Himalaya using remote-sensing data and distributed hydrological modeling. *Advances in Water Resources*, *88*, 152–169. https://doi.org/10.1016/j.advwatres.2015.12.004

Xu, Q., Hoke, G. D., Liu-Zeng, J., Ding, L., Wang, W., & Yang, Y. (2014). Stable isotopes of surface water across the Longmenshan margin of the eastern Tibetan Plateau. *Geochemistry*, *Geophysics*, *Geosystems*, *15*(8), 3416–3429. https://doi.org/10.1002/2014GC005252

Yu, W., Yao, T., Tian, L., Ma, Y., Wen, R., Devkota, L. P., … Chhetri, T. B. (2016). Short-term variability in the dates of the Indian monsoon onset and retreat on the southern and northern slopes of the central Himalayas as determined by precipitation stable isotopes. *Climate Dynamics*, *47*(1–2), 159–172. https://doi.org/10.1007/s00382-015-2829-1

SUPPORTING INFORMATION

Additional supporting information may be found online in the Supporting Information section at the end of the article.

How to cite this article: Meese B, Bookhagen B, Olen SM, Barthold F, Sachse D. The effect of Indian Summer Monsoon rainfall on surface water δD values in the central Himalaya. *Hydrological Processes*. 2018;32:3662–3674. https://doi.org/10.1002/hyp.13281